RSC Advances

PAPER

View Article Online
View Journal | View Issue

Cite this: *RSC Adv.*, 2021, **11**, 14334

Insights into the climate-driven evolution of gas hydrate-bearing permafrost sediments: implications for prediction of environmental impacts and security of energy in cold regions†

Mehrdad Vasheghani Farahani, [a] Aliakbar Hassanpouryouzband, [ab] Jinhai Yang *[a] and Bahman Tohidi[a]

The present study investigates the evolution of gas hydrate-bearing permafrost sediments against the environmental temperature change. The elastic wave velocities and effective thermal conductivity (ETC) of simulated gas hydrate-bearing sediment samples were measured at a typical range of temperature in permafrost and wide range of hydrate saturation. The experimental results reveal the influence of several complex and interdependent pore-scale factors on the elastic wave velocities and ETC. It was observed that the geophysical and geothermal properties of the system are essentially governed by the thermal state, saturation and more significantly, pore-scale distribution of the co-existing phases. In particular, unfrozen water content substantially controls the heat transfer at sub-zero temperatures close to the freezing point. A conceptual pore-scale model was also proposed to describe the pore-scale distribution of each phase in a typical gas hydrate-bearing permafrost sediment. This study underpins necessity of distinguishing ice from gas hydrates in frozen sediments, and its outcome is essential to be considered not only for development of large-scale permafrost monitoring systems, bus also accurate quantification of natural gas hydrate as a potential sustainable energy resource in cold regions.

Received 24th February 2021
Accepted 9th April 2021

DOI: 10.1039/d1ra01518d

rsc.li/rsc-advances

1. Introduction

Gas hydrates are ice-like crystalline nonstoichiometric compounds comprised of suitably sized gas molecules, predominantly methane, enclosed within a solid lattice of water molecules.[1,2] They form where there is a sufficient supply of water and gas at favorable thermodynamic conditions of high pressure and low temperature.[3] Huge volumes of natural gas hydrates are deposited along the continental shelf and slope regions, and in permafrost areas, inland seas and freshwater lakes.[4] Given their remarkable gas storage capacity and abundant occurrence in nature, gas hydrate-bearing sediments are potentially regarded as low carbon energy resources in the near future.[5,6] Tremendous research effort has been conducted so far to tackle technical and economic hurdles in order to develop commercially viable and environmentally friendly exploitation techniques.[7–9] Furthermore, injection of CO_2 or CO_2-contained mixtures into gas hydrate-bearing sediments is a promising and efficient technique for simultaneous methane recovery and direct capture and storage of CO_2.[10–14] From a different perspective, however, gas hydrate-bearing sediments play an important role in the global carbon cycle influencing the Earth's climate,[15] as methane is 20–30 times more potent as a greenhouse gas than CO_2.[16] Ocean and atmospheric warming may disturb the thermal stability of hydrates, resulting in hydrate dissociation and methane release into the marine environment and overlying sediments.[17] Methane and methane-derived carbon may eventually reach the atmosphere and exacerbate the greenhouse effect. This, in turn, could impend further temperature rise which drives releasing the enormous reserves of methane, leading to a circular reaction which would accelerate global warming.[18] Nevertheless, methane release from hydrate-bearing sediments is believed to be slow and chronic rather than catastrophic at present, because of several mitigating factors such as the depth and thickness of the hydrate stability zone, strong sediment and water column sinks and inability of methane bubbles seeped into the seafloor to reach the atmosphere.[17,19] Global warming together with seasonal changes and anthropogenic activities, however, could be still unfavorable given gas hydrate stability is extremely sensitive to temperature.[20] Gas hydrate dissociation may substantially alter physical properties of the host sediment, particularly its geothermal and mechanical characteristics, resulting in serious geohazards such as sediment deformation and slides and

[a]*Hydrates, Flow Assurance & Phase Equilibria Research Group, Institute of GeoEnergy Engineering, Heriot-Watt University, Edinburgh, EH14 4AS, UK. E-mail: petjy@hw.ac.uk*
[b]*School of Geosciences, University of Edinburgh, Grant Institute, West Main Road, Edinburgh, EH9 3JW, UK*

† Electronic supplementary information (ESI) available. See DOI: 10.1039/d1ra01518d

submarine slope failure in continental margins.[16] It may also cause wellbore instability during drilling and casing deformation/collapse during production through gas hydrate-bearing zones.[21] In regions underlain by ice-rich permafrost, ice thawing and hydrate dissociation could induce settlement of the ground surface and severely damage human infrastructure.[22]

Ice and gas hydrates both have similar elastic moduli.[23] Therefore, the presence of hydrates enhances the skeletal stiffness of the host sediment and consequently, results in higher elastic wave velocities.[24] This feature has led a tremendous number of field-scale studies, mainly aiming at mapping and quantifying gas hydrates in oceanic and terrestrial sediments using seismic techniques, a detailed review in this regard can be found elsewhere.[2] Given the conventional exploration techniques primarily rely on the evolution of geophysical response of gas hydrate-bearing sediments, considerable work has been conducted in laboratory to investigate the pore-scale processes accompanying hydrate formation in porous media in order to understand how hydrates alter the skeletal properties of the host sediment and influence the magnitude of the compressional (P) and shear (S) wave velocities.[25] Various empirical and physics-based methods have been also developed to establish a relationship between the elastic wave velocities and hydrate saturation, and thereby predict the physical properties of gas hydrate-bearing sediments.[26] However, there is still lack of fundamental knowledge regarding the pore-scale phenomena influencing the physical properties of permafrost, particularly gas hydrate-bearing permafrost sediments compared to merely frozen or hydrate-bearing unfrozen sediments.[20] The biggest challenge is that the seismic techniques fail to distinguish gas hydrates from ice due to their similar acoustic properties. In addition, it is not possible to mark permafrost-associated gas hydrates since bottom simulating reflectors (BSRs) are not likely to occur in permafrost settings.[17,27]

Thermal evolution of permafrost is governed by coupled thermal-hydrological processes on the surface and in the subsurface.[28] Thus, the performance of permafrost modeling approaches in different applications such as permafrost proneness modeling and freezing soil evolution modeling essentially depends on the thermal and hydraulic conductivities fitted to the model. These physical properties depend not only on the saturations of the co-existing phases, but also their pore-scale distribution and interfacial effects.[2] In our recently published study, we have shown that the heat transfer in unsaturated porous medium is a complex phenomenon affected by several important pore-scale mechanisms. In particular, we discussed how the effective thermal conductivity (ETC) is influenced by the co-existence of ice, unfrozen water, and gas at frozen conditions.[29] It should be noted that the presence of different minerals (silt, clay, …) and their interaction with pore water influence not only the physical properties of the host sediment, but also the pore-scale distribution of the co-existing phases in pore space,[40] particularly at frozen conditions, where the unfrozen water content occupying small pores critically contributes to the heat tranfer.[29] The presence of hydrates adds further complexities, which is required to be well understood and accounted for in both lab- and field-scale studies; otherwise, the prediction of the thermal response of gas hydrate-bearing permafrost sediments would be erroneous. Interestingly, ETC is the physical property which could be sufficiently used to describe the unique features of gas hydrate-bearing permafrost sediments and particularly, distinguishing gas hydrates and ice from each other at frozen conditions. The reason is that (i) ETC depends on the intrinsic thermal conductivity and volume fraction of each individual constituent as well as the pressure, temperature, porosity, and grain packing structure[30] and (ii) the intrinsic thermal conductivity of gas hydrates is almost four times lower than that of ice.[31] Although ETC of gas hydrate-bearing sediments has been extensively investigated at unfrozen conditions, little work has been carried out at frozen conditions to the best of our knowledge.[32–35] There is also another challenge when investigating the thermal response of natural gas hydrate-bearing sediments: how to distinguish methane hydrates from water despite their quite similar intrinsic thermal conductivity values.[23]

In this article, we report experimental measurements of the elastic wave velocities and ETC of methane hydrate-bearing permafrost sediment samples at a typical range of temperature in permafrost and different hydrate saturations (up to 60%). The primary aim is to develop a profound understanding of the pore-scale phenomena influencing the climate-driven evolution of gas hydrate-bearing permafrost sediments. Our particular interest is on the co-existence of hydrates, ice, unfrozen water, and free gas at different sub-zero temperatures to explain how they contribute to the evolution of the acoustic and thermal properties of the host sediment. A conceptual pore-scale model will be also developed to describe gas hydrate-bearing permafrost sediments at both unfrozen and frozen conditions based on their measured elastic waves and ETC. Ultimately, a detailed discussion will be provided regarding the potential contribution of this study on the prediction of the environmental impacts and energy security in cold regions.

2. Experimental section

2.1. Materials

Research-grade methane and N_2 with certified purities of 99.995 vol% were supplied by BOC Limited. Deionized water was produced using an Integral Water Purification System (ELGA DV 25). A well-characterized silica sand from Fife, Scotland was used as the porous media. The silica sand has a density (ρ_s) of 2.64 g cm^{-3}, particle sizes ranging from 1.2 to 600 μm, and a mean diameter of 256.5 μm.[36]

2.2. Experimental apparatus

Two high-pressure cylindrical cell setups were employed to conduct the experiments. The schematic diagram of the setup used for the measurement of the elastic wave velocities is depicted in Fig. 1. The configuration is the same for the other apparatus except the cell is equipped with a needle probe for measurement of ETC (see ref. 29). Each setup consists of a high-

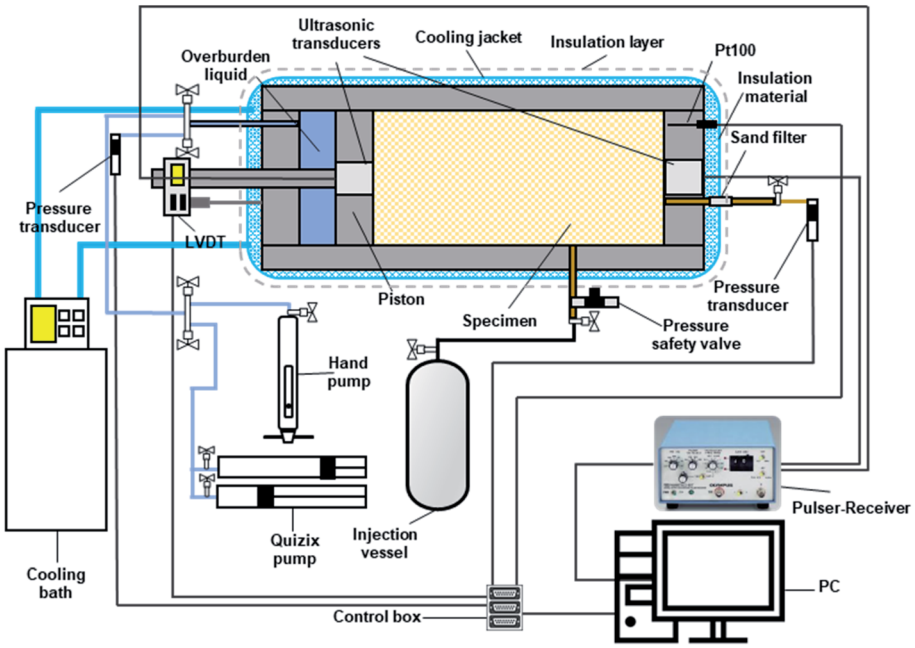

Fig. 1 Schematic diagram of the high-pressure setup used for measurement of the elastic wave velocities. The configuration for the setup used for measurement of ETC is the same except a needle probe is mounted on the fixed endcap of the cell instead of the ultrasonic transducers.

pressure 316 stainless steel cell (maximum working pressure of ~42 MPa, inner diameter of 75 mm and inner length of 150 mm), movable piston, pressure/temperature maintaining unit and data measurement and acquisition unit. The movable piston was installed at one end of the cell and driven by the hydraulic pressure exerted behind by a Quizix pump (SP-5200, Vindum Engineering Inc., USA) with dual cylinders to keep specimen compacted at a desired effective overburden pressure. A linear variable differential transmitter (LVDT) was also mounted on the piston rod to determine its position, enabling us to calculate the instantaneous volume hence the porosity of the specimen. The cell is surrounded by an integral cooling jacket connected to a cryostat to maintain the system temperature at a desired value. A platinum-resistance thermometer with a precision of ±0.1 °C (Pt100, TC Ltd) was also coated in the cell to measure the system temperature. Two calibrated Druck pressure transducers with an accuracy of ±0.05 MPa were used to measure the pore and overburden pressures, respectively. As shown in Fig. 1, the cell has two ports, one at the side for the gas injection and the other one at the fixed endcap connected to the pressure transducer to measure the pore pressure. The pore pressure, temperature, overburden pressure, and piston displacement were continuously monitored at regular time intervals and recorded using a data acquisition module (LabVIEW software, National Instruments).

2.3. Experimental procedure

Each test specimen was made by mixing the silica sand and deionized water at a predetermined mass ratio of 14.46 wt%, rendering an initial water saturation of nearly 60%. The cell was then filled with the partially saturated specimen and vacuumed after adjusting the piston level to control the volume. When loading the cell, the specimen was regularly tamped to achieve a uniform compaction. Thereafter, a hydraulic pressure of 3.45 MPa was applied behind the piston initially with the hand pump and maintained using the Quizix pump to further compact the specimen. The effective overburden pressure of 3.45 MPa is a typical value for sediments in permafrost with a porosity of 0.38–0.40 (see ref. 26). The system was then left at 20 °C for at least 12 hours to reach the thermodynamic equilibrium. Methane was then injected until the pore pressure reached the desired value while keeping the effective overburden pressure constant (N_2 was injected for the hydrate-free case). The system was left again for at least 12 hours at this condition until the pressure and temperature of the system became stable and no piston movement was observed. Eventually, the temperature was set to 3.0 °C (T_1) to form hydrates. After the system reached the equilibrium thermodynamic conditions, the specimen underwent the elastic wave velocities or ETC measurement. Then the system temperature decreased to 0.5 (T_2), −0.5 (T_3), −3.0 (T_4) and −9.0 °C (T_5) in steps and the measurements were carried out at both unfrozen and frozen conditions. It should be noted that there was no elastic wave velocity measurement below −3.0 °C due to the working temperature limit of the ultrasonic transducers. When unloading the cell, three samples were taken from different portions and their water saturation was measured to examine the homogeneity of the system throughout the measurements.

The P- and S-wave velocities were measured using a pair of combined ultrasonic transducers (Panametrics, central frequency: 1 MHz) embedded into the fixed endcap and piston, respectively. A pulser-receiver (Panametrics, 5077PR) was employed to send the signals from the transmitting transducer

to the receiving one. The waveforms were visualized and recorded using a DSO oscilloscope that was connected to a PC for analysis. The elastic wave velocities were measured using the ultrasonic transmission method which requires accurate measurements of the travel time (t) of the elastic waves together with the propagation distance through the specimen (L).[25] Having the inherent travel time (t_0) of both P- and S-waves, the velocity (v) could be calculated according to eqn (1):

$$v_i = \frac{L}{t_i - t_{0i}} \quad (1)$$

where i stands for P and S.

Transient hot wire method was employed for the ETC measurements. In this method, the needle probe, as a long and thin heating source, is inserted into the specimen, heated with a constant power (*via* applying certain current and voltage to the probe), and the temperature rise inside the source is recorded *versus* time. Thermal conductivity is obtained *via* analyzing the temperature time series data during the heating cycle using eqn (2):

$$\Delta T \cong \frac{Q}{4\pi\lambda} \ln(t) \quad 0 < t < t_1 \quad (2)$$

in which λ, Q, ΔT, t, and t_1 are the thermal conductivity, applied heat per unit length of the needle probe, temperature change, measuring time, and heating time.[29] A detailed discussion regarding the test method can be found elsewhere.[29,37] The ETC measurements were carried out using a calibrated purpose-built needle probe (TP08, Hukseflux, The Netherlands) which can accurately measure the thermal conductivity at elevated pressures in compliance with the ASTM D5334-14 standard.[37] The thermal conductivity data were recorded in a measurement and control unit connected to a PC. It should be noted that the measurements were repeated to eliminate the experimental data contingencies. The total heat to the specimen was also adjusted by setting the heating duration to impose a small temperature gradient hence avoid any phase change around the needle probe.

The experimental errors of the elastic wave velocities and ETC measurements were reported together with the experimental data. The procedure followed for estimation of the experimental measurement errors was also detailed in ESI.†

2.4. Saturation calculations

The instantaneous porosity (ϕ) of the specimen was determined according to eqn (3):

$$\phi = 1 - \frac{m_s}{V_b \rho_s} \quad (3)$$

where m_s and ρ_s are the mass and density of the dry silica sand particles, respectively and V_b is the bulk volume calculated according to the diameter (D) and instantaneous length of the specimen (l). The volumes of hydrate (V_h), water (V_w), and gas (V_g) were also calculated as follows:

$$V_h = \frac{W_h n_h}{\rho_h} \quad (4)$$

$$V_w = \frac{W_w}{\rho_w}(n_{w,initial} - n_h\gamma) \quad (5)$$

$$V_g = \overline{V}_g(n_{g,initial} - n_h) \quad (6)$$

W_h, W_w, ρ_h and ρ_w stand for the molecular weights and densities of methane hydrate and water, and $\bar{V}_g$ is the methane specific volume. W_h is calculated by eqn (7):

$$W_h = W_g + \gamma W_w \quad (7)$$

where γ is the hydration number and W_g is the molecular weight of methane. $n_{g,initial}$ and $n_{w,initial}$ are the numbers of moles of the methane injected and initial water content. It should be noted that water was assumed completely frozen at sub-zero temperatures hence ρ_w was substituted by the ice density (ρ_i) in eqn (5) to account for the volume expansion due to the transformation of pore water to ice. Table 1 presents the values of the parameters used in eqn (4)–(7).

Values of ρ_h, γ and $\bar{V}_g$ were also determined for each individual data point using our in-house PVT modelling software[38] and are available in ESI.† Having the instantaneous pore volume ($V_p = \phi V_b$), eqn (8) could be solved to obtain the number of moles of methane hydrate (n_h):

$$V_p = V_h + V_w + V_g \quad (8)$$

The instantaneous volume of each phase was then calculated using eqn (4)–(6). The volumetric saturation of hydrate (S_h), water (S_w), and gas (S_g) were found using eqn (9):

$$S_i = \frac{V_i}{V_p} \quad i: \ h, \ w, \ g \quad (9)$$

3. Results and discussion

3.1. Analysis of the evolution of the elastic wave velocities

Fig. 2 illustrates the measured elastic wave velocities of the hydrate-free and hydrate-bearing permafrost sediment samples *versus* the system temperature at different hydrate saturations. At unfrozen conditions, the presence of hydrates results in higher P- and S-wave velocities whereas the pore fluids (free gas and water) cannot exhibit such a significant influence. This is expected because the bulk modulus of the pore fluids is markedly lower than that of methane hydrates and their shear modulus is zero (S-wave cannot propagate through fluids).[23] Moreover, the presence of hydrates stiffens the host sediments, leading to higher elastic wave velocities. It can also be seen that

Table 1 Parameters used for the saturation calculations

No.	Parameter	Value	Unit
1	W_g	16.04	g mol^{-1}
2	W_w	18.02	g mol^{-1}
3	ρ_w	1.00	g cm^{-3}
4	ρ_i	0.92	g cm^{-3}

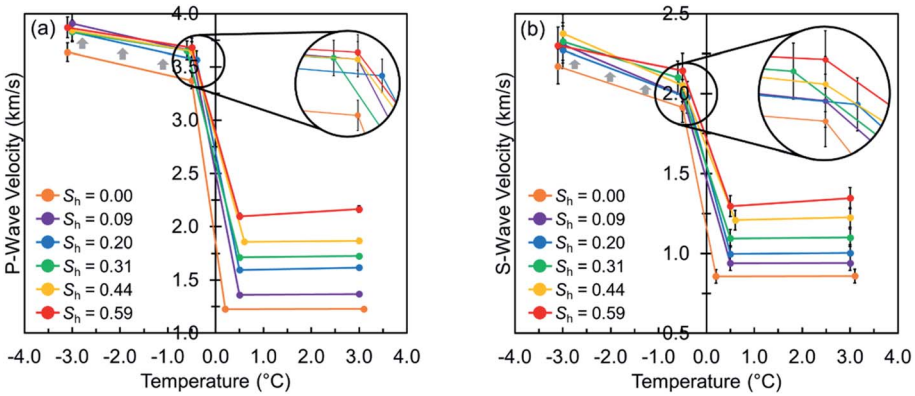

Fig. 2 (a) P-wave and (b) S-wave velocities against the system temperature.

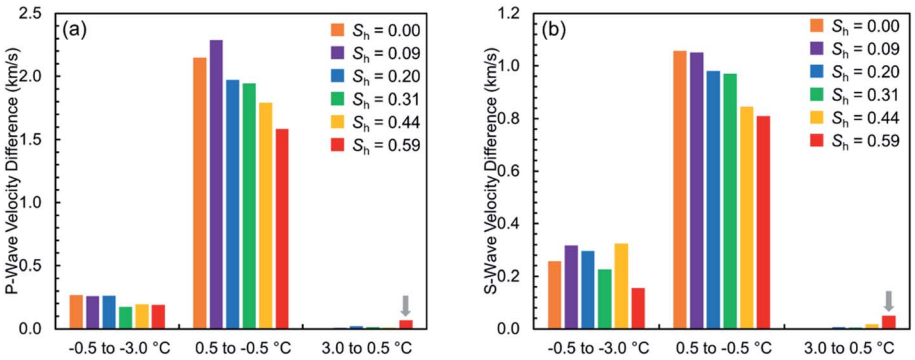

Fig. 3 Variations in (a) P-wave and (b) S-wave velocities with the system temperature.

the system temperature generally has no strong effect on the elastic wave velocities. When the system temperature goes below the freezing point, transformation of a portion of pore water to ice leads to a drastic increase in the elastic wave velocities, which in contrast to the unfrozen conditions, is influenced by the system temperature. The underlying reason is that the amount of the unfrozen water content is essentially controlled by the system temperature.[39] Therefore, further freezing results in more transformation to ice hence higher elastic wave velocities.

The presence of hydrates at frozen conditions, even at low saturations, results in shifting the P- and S-wave velocities toward elevated values, away from those of the hydrate-free case (see gray arrows in Fig. 2). Such behavior might make no sense at first glance since an identical initial water content was considered for all experiments and water at frozen conditions must have been either trapped in the hydrate crystals, transformed to ice, or remained unfrozen, depending on the temperature and hydrate saturation. Therefore, the elastic wave velocities of the hydrate-free and hydrate-bearing sediment samples would have been expected to be relatively close at frozen conditions, which is in contrast with what observed in Fig. 2. This interesting behavior could be attributed to the effect of development of hydrate micro-frame structures throughout the specimen. We observed similar behavior in our recent study, where the distinctive effect of gas hydrates and ice on the geomechanical properties of hydrate-bearing and hydrate-free permafrost sediments was investigated.[20] The hydrate micro-frame structures may develop in partially saturated sediments, where pore water forms a film around the sediment grains, depending on their mineralogy and wettability characteristics, and builds up a water network.[40] In such a porous medium, ice is expected to form in the large pores due to the cryosuction[41] and cement the sediment grains mainly at the vicinity of their contact regions.[20] However, hydrate is expected to nucleate at the gas–water interface throughout the system,[42] making the methane gas bubbles formerly surrounded by pore water to gas-filled or solid methane hydrate bars. Local growth and extension of these hydrate bars may create the hydrate micro-frame structure, reinforcing the stiffness of the host sediment, leading to higher elastic moduli and consequently, shifting the elastic wave velocities toward the elevated values.

Fig. 3 shows the absolute variations in the measured elastic wave velocities of the hydrate-free and hydrate-bearing permafrost sediment samples ($|v_i^{T_j} - v_i^{T_{j+1}}|$, i: P/S, j: 1, 2, 3). It is observed that the increase in the elastic wave velocities from 0.5 to −0.5 °C is higher in the hydrate-free sediment sample than in the hydrate-bearing ones. The underlying reason is the fact that there is a higher amount of water available to get frozen at the hydrate-free case, particularly at the large pores where the ice nucleation occurs first in due to the cryosuction.[41] In addition, gas hydrate tends to start nucleating at these large pores where

more nucleation sites with gas–water interface are available[20,26] hence there would be relatively less water available in the large pores to contribute toward increasing the elastic wave velocities of hydrate-bearing sediments when the system temperature goes below the freezing point. Even though this effect might not be clear enough when investigating the variations in P-wave velocity solely as unfrozen water still contributes to the P-wave velocity values, the variations in S-wave velocity could assist with as S-wave can only be influenced by the sedimentary matrix of sand particles, ice and methane hydrates.

3.2. Analysis of the evolution of the effective thermal conductivity

Fig. 4 presents the measured ETC values of the hydrate-free and hydrate-bearing permafrost sediment samples *versus* the system temperature at different hydrate saturations. At unfrozen conditions, it can be seen that the measured values at 0.5 °C are slightly lower than those at 3.0 °C for all hydrate saturations, mainly due to the fact that the intrinsic thermal conductivity of all constituents is positively correlated with temperature,[1,2,43,44] hence the lower the system temperature, the lower the intrinsic thermal conductivity. In addition, the convective heat transfer mechanism in the pore fluids could diminish at lower temperatures. When the system temperature goes below the freezing point, transformation of a portion of pore water to ice results in an increase in ETC. Even though the intrinsic thermal conductivity of ice is almost four times greater than that of water, it is observed that the increase in the ETC values is not dramatic at −0.5 °C. This behavior could be attributed to the cryosuction, which results in the critical pathways essentially controlling the intergranular heat transfer in the system to be still occupied by unfrozen water.[41,45] In fact, there are ice crystals in the system, however, they still have no well-developed network hence the heat transfer is curtailed due to the high thermal contact resistance (TCR). Further freezing to −3.0 °C, however, leads to transformation of a higher amount of unfrozen water to ice, and consequently, lower TCR and more efficient heat conduction. We also observed a slight decrease in the ETC values at −9.0 °C, which could be attributed to the ice-forced heave.[34] It should be noted that the transformation of pore water to ice for the hydrate-free case was associated with a volume expansion, resulting in a less than 1.0 MPa increase in the pore pressure (see ESI†). However, the dependence of ETC on the pore pressure is not strong,[29] hence we would not expect a measurable effect originating from the pore pressure on ETC of the gas hydrate-free sediment sample when a portion of pore water gets frozen. For the gas hydrate-bearing cases, the pore pressure of the system is essentially controlled by the methane hydrate phase boundary, hence we would not expect any pore pressure increase when the system temperature goes below the freezing point.

We performed further ETC measurements for the hydrate-free sediment sample at temperatures between −0.5 and −3.0 °C to explore how ETC changes as a result of the water transformation to ice. As observed in Fig. 4a, ETC of the specimen does not increase monotonously and experiences two stages of the elevation. Such behavior could be understood based on unification of the thermal conductivity behavior and soil water retention mechanisms.[40] According to our recent experimental study on ETC of hydrate-free partially saturated sediments, the volumetric water saturation of 58% means that the water distribution in our sediment samples could be described by the funicular retention regime (see Fig. 4b).[29] In this regime, water films form around the sediment grains and build up a water network. Water in this network does not influence ETC as critically as water in the small pores (referred as the pendular regime). Therefore, it would not be expected that ice crystals formed from pore water in the funicular regime have a huge contribution to the ETC elevation.

3.3. Effect of the saturation and pore-scale habit of hydrates

The experimental results clearly demonstrate that the evolution of the geophysical response of gas hydrate-bearing permafrost sediment samples at both unfrozen and frozen conditions essentially depends on the saturation and pore-scale habit of hydrates. At unfrozen conditions, it can be seen in Fig. 2 that the presence of hydrates at saturations less than 0.31 does not significantly affect the elastic wave velocities because the

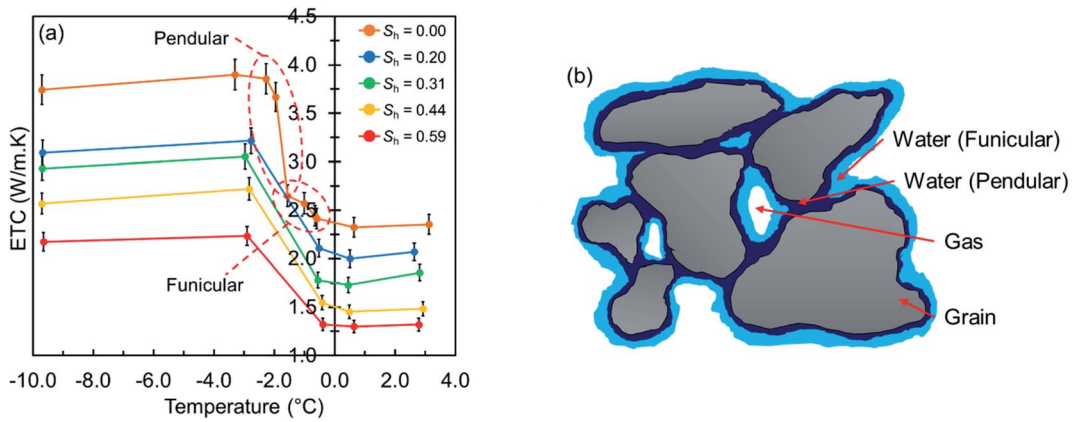

Fig. 4 (a) Measured ETC values against the system temperature, (b) typical pore-scale distribution of water in an unsaturated sediment without clay content. The retention regime of capillary is expected at higher water saturations.[40]

dominant pore-scale habit of hydrates is expected to be pore-filling.[23] However, as the hydrate saturation increases, dominance of the pore-scale habit changes toward load-bearing, hence the hydrate contribution to the skeletal stiffness becomes significant, leading to a higher elevation in the elastic wave velocities. Another interesting observation is that P-wave velocity is somewhat more sensitive to the thermodynamic conditions than S-wave velocity at higher hydrate saturations (see Table 2 and gray arrows in Fig. 3). Such a behavior could be attributed to the sensitivity of the elastic bulk moduli of the pore fluids to the thermodynamic conditions at different hydrate saturations. First, it is a given that S-wave propagates only through the solid contents (*i.e.* sand particles and hydrates) whose elastic moduli are almost not sensitive to temperature, while the propagation of P-wave is influenced by the pore fluids in addition to the solid matrix.[23] Moreover, changes in the saturation of different phases in the sediment samples show that the volume occupied by hydrates is provided primarily by pore water (see ESI†). Therefore, at higher hydrate saturations, pore water would be replaced by hydrates and the contribution of the pore fluids to the P-wave velocity value become dominated by free gas, the constituent with the most sensitive elastic bulk modulus to the thermodynamic conditions.[46] However, we believe further investigation with more accurate ultrasonic transducers is necessary to understand this behavior, particularly at low hydrate saturations with dominance of water in the pore fluid contribution to the P-wave velocity.

At frozen conditions, the elastic wave velocities exhibit no consistent trend as a function of the hydrate saturation which evidently indicates why the conventional seismic techniques cannot quantify gas hydrates in permafrost. It should also be noted that the elastic wave velocities are slightly higher for the sediments with more hydrate saturations at −0.5 °C, which could be attributed to the effect of the unfrozen water content. As discussed earlier, there would be less water available to get frozen for sediment samples with higher hydrate saturations.

As previously discussed, ETC could assist with distinguishing ice from gas hydrates; however, the heat transfer in porous media is a complex phenomenon governed by several pore-scale mechanisms and the interaction of different co-existing phases adds further complexities.[47] It is observed that ETC decreases as the hydrate saturation increases at both unfrozen and frozen conditions. At unfrozen conditions, such behavior could be attributed to three main factors: (i) the intrinsic thermal conductivity of methane hydrates is slightly lower than that of water,[48,49] (ii) the heat transfer in the hydrate–gas interface is less efficient than in water–gas interface due to the fact that the mass transfer in a fluid–fluid interface may facilitate the energy transfer,[29] (iii) the sand particles could be rearranged by hydrates at higher saturations where the dominant pore-scale habit is load-bearing and the hydrate crystals could push apart the sediment grains, a phenomenon known as hydrate-forced heave, which could result in enlarging the sediment pores and increasing TCR.[5] At frozen conditions, it is observed that ETC decreases when the hydrate saturation increases because less water is available to turn into ice at higher hydrate saturations. This behavior can also be seen when investigating the evolution of the ETC values from −0.5 to −3.0 °C, the higher the hydrate saturation, the lower the increase in ETC of the sediment sample, particularly at the hydrate saturation of 51% where the pore-scale habit is load-bearing and the contribution of the hydrate micro-frame structure to the heat transfer becomes significant.

Fig. 5 illustrates the measured values of elastic wave velocities and ETC against the methane hydrate saturation at unfrozen and frozen conditions. The velocity ratio v_P/v_S is plotted *versus* the methane hydrate saturation in Fig. 6 to investigate how the acoustic properties of the sediment samples varied with the hydrate saturation. The velocity ratios are all less than 2, indicating either the presence of gas in an unconsolidated sand – which is valid for the results at unfrozen conditions – or a well-consolidated sediment – which is also valid for the results at frozen conditions (see ref. 50 for further discussion).

At unfrozen conditions, it can be seen in Fig. 5a that the elastic wave velocities are sensitive to the methane hydrate saturation, which makes it possible to determine the hydrate saturation using the geophysical models available in the literature. At frozen conditions, Fig. 5b demonstrates that ETC distinctly captures the co-existence of ice and hydrates. As previously discussed, ETC can also account for the effect of the unfrozen water content and reflect the dominant pore-scale habit of hydrates. This is why ETC could considerably assist with when attempting to obtain the hydrate saturation and understand the pore-scale distribution of all co-existing phases at frozen conditions. However, care must be taken when analyzing the thermal properties as they are essentially influenced by several pore-scale mechanisms controlling the heat transfer through porous media.[45] Fig. 6 shows that the velocity ratio generally tends to decrease gradually as a function of the hydrate saturation at both −0.5 and −3.0 °C while still be influenced by the amount of unfrozen water. Therefore, although the changes in the velocity ratio is fairly small, it could be used as an additional geophysical parameter to assist with determination of the unfrozen water content.

Table 2 Absolute variations in the measured elastic wave velocities from 3.0 to 0.5 °C

	S_h (—)					
Absolute variation (km s^{-1})	0.00	0.09	0.20	0.31	0.44	0.59
Variation in P-wave	0.003	0.008	0.021	0.012	0.010	0.068
Variation in S-wave	0.002	0.001	0.006	0.005	0.017	0.050

4. A conceptual model for gas hydrate-bearing permafrost sediments

Our experimental results confirm that the physical properties of gas hydrate-bearing permafrost sediments are greatly influenced by the co-existence of hydrates, ice, water and free gas. Therefore, it is essential to account for the complexities

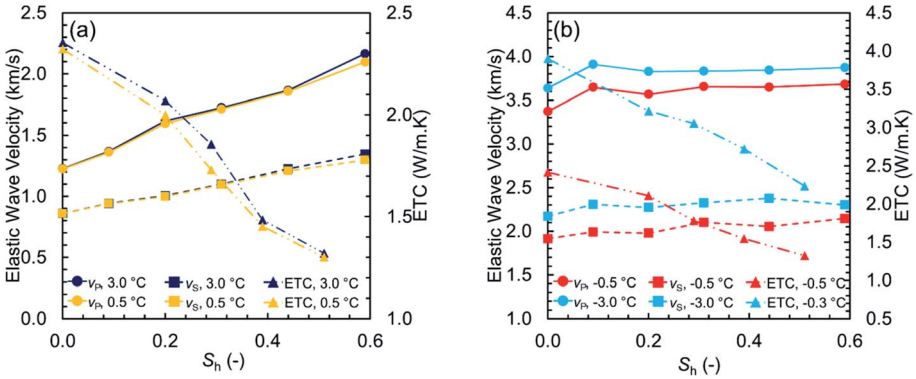

Fig. 5 The measured values of the elastic wave velocities and ETC *versus* the methane hydrate saturation at (a) unfrozen and (b) frozen conditions.

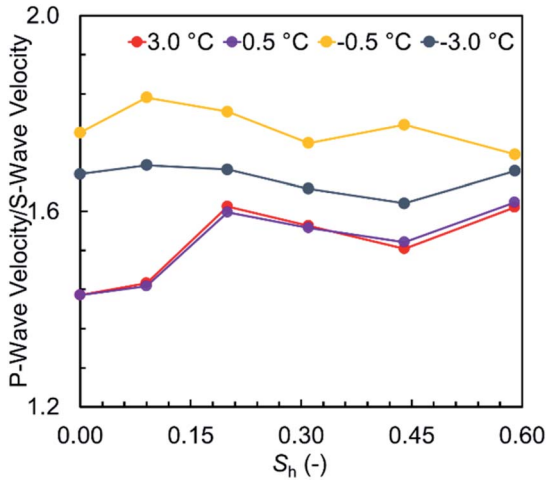

Fig. 6 Dependence of v_P/v_S on the volumetric methane hydrate saturation at unfrozen and frozen conditions.

associated with the interaction of the co-existing phases with each other and the host sediment in order to be able to accurately predict their response to the environmental temperature change. However, to the best of our knowledge, available models in the literature are unable to achieve this since they cannot successfully take into consideration the effect of the unfrozen water content and distinguish gas hydrates from ice at frozen conditions. In this section, we propose a conceptual pore-scale model for gas hydrate-bearing permafrost sediments based on their geophysical and geothermal responses to the changing temperature. To be in accordance with our findings in this study, we assume a sandy porous medium with the same initial water content, described by the funicular retention regime, for both hydrate-free and hydrate-bearing cases at different thermal states. These assumptions are necessary because presence of the other grain types with different mineralogy, size, and wettability characteristics (*e.g.* silt and clay) as well as the pore-scale distribution of water (which depends on its initial saturation and interaction with the host sediment) control the kinetics of formation, saturation, and spatial distribution of hydrate crystals in pore space,[9] hence may even add further complexities to the system. Future experimental studies with a focus on the effect of the water content and the sediment mineralogy will be required to be conducted to complete this work, and their outcomes could be incorporated into the model.

Fig. 7 schematically depicts the pore-scale distribution of the co-existing phases in a typical gas hydrate-bearing permafrost porous medium with different hydrate saturations at both unfrozen and frozen conditions. As observed, the sediment grains are in contact with each other and essentially coated with a layer of water due to their hydrophilic characteristics. The contact area between the neighboring grains depends on several factors such as the grain size, shape, elastic moduli and the effective overburden pressure.[51] Moreover, the thickness of the water layer is controlled by the initial water saturation (prior to the hydrate and ice formation), pore size, capillary pressure, thermal state and the existence of the other phases such as hydrates.[52]

At unfrozen conditions, the hydrate nucleation and growth tend to occur at the large pores, far from the grain contacts, where the gas–water interface, as the most possible site for hydrate nucleation, is available.[42] The presence of gas hydrates (a solid constituent with an elastic bulk modulus almost four times greater and an intrinsic thermal conductivity slightly lower than those of water) in pores results in elevation of the elastic wave velocities and slight decrease in ETC. The magnitude of the evolution of the elastic wave velocities and ETC values greatly depends on the hydrate saturation and pore-scale habit. At lower hydrate saturations where pore-filling is the dominant pore-scale habit, the hydrate crystals are suspended in pore water hence their influence would be only on the stiffness and thermal conductivity of the pore-fluid. At higher hydrate saturations where the dominant pore-scale habit alters to load-bearing, hydrates can grow and extend across grains, create micro-frame structure throughout the host sediment and reinforce it. However, the hydrate-forced heave could also take place at higher hydrate saturations, in which hydrate crystals push apart the sediment grains, reduce the contact area between the neighboring grains, and adversely influence the heat transfer.

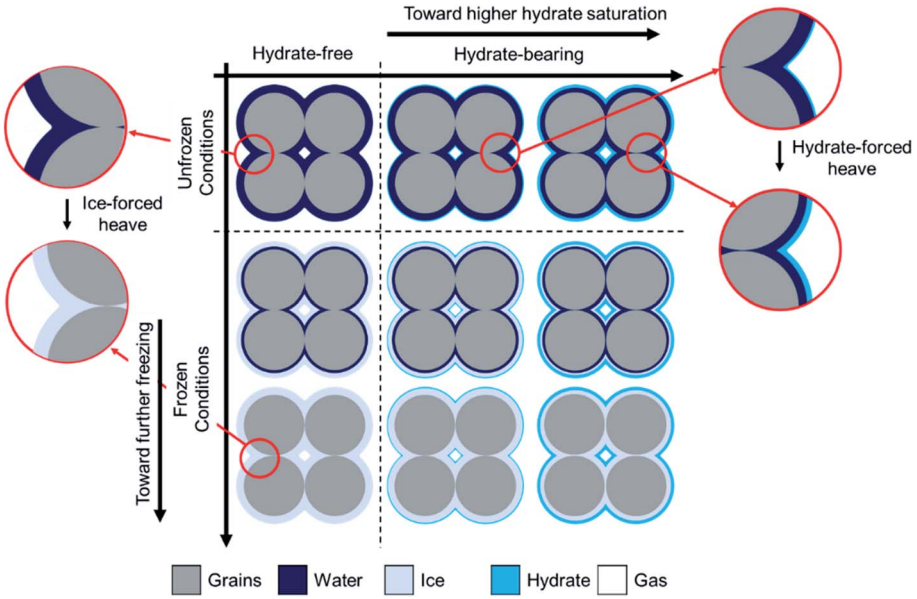

Fig. 7 Schematic of the hypothetical pore-scale distribution of water and/or ice together with hydrates in permafrost sediments.

At frozen conditions, water in the large pores (capillary and funicular regimes) starts to turn into ice, a constituent with the elastic moduli similar to those of gas hydrates and intrinsic thermal conductivity almost four times greater than that of water. The hydrate saturation controls the amount of water available for freezing in this regime. At temperatures close to the freezing point, the presence of ice substantially enhances the elastic moduli of the host sediment, leading to a drastic increase in the elastic wave velocities. Nevertheless, the small pores which critically contribute to the heat transfer are still occupied with unfrozen water, resulting in no sharp increase in ETC of the sediment (see section 3.2). Further freezing leads to transformation of water in the small pores (pendular regime) to ice hence higher contribution to the heat transfer. However, as discussed previously, this could result in the ice-forced heave which adversely influences the thermal conduction by reducing the contact area between the neighboring grains and increasing TCR.

It should be noted that further experimental studies are required to be conducted in order to understand how the hydrate and/or ice-forced heave may affect the contact area between the neighboring sediment grains and accordingly, the contribution of the grain–grain conduction to the heat transfer in gas hydrate-bearing permafrost porous media. As discussed in section 3, this effect depends on the thermal state of the system as well as the saturation and pore-scale distribution of the co-existing phases. *In situ* observation techniques such as X-ray micro-CT imaging may assist with shedding light on this interesting and complex phenomenon.

5. Implications

Cold environments, characterized by the presence of permafrost and extensive snow and ice cover, are important ecosystems, creating various development opportunities for economic growth such as mineral extraction and energy exploitation. However, these areas are quite sensitive to climate change and prone to human activities. A profound understanding of thermal evolution of these partly or fully frozen regions is necessary for accurate evaluation and prediction of impacts of climate change and/or potential development scenarios on their geophysical, geothermal, and hydrological responses. Permafrost is considered as a low permeability physical barrier to upward migration of gases from the subsurface.[53] The strong amplification of global warming as a result of the pronounced greenhouse effect, accelerates the thawing rate of permafrost at Arctic regions, potentially leading to enhanced methane emission from current permafrost areas over the land and Arctic ocean.[54] On the other side of the coin, submarine groundwater discharge may largely influence the extent of submarine permafrost and gas hydrate stability.[55] This interplay may endanger ecosystems and infrastructures at the local and regional scale by limiting resource development and fragmenting ecosystems.

Presently, the Arctic regions are warming at twice the global average rate,[56] resulting in pronounced snow cover and sea ice decline, permafrost degradation, and lake and wetland expansion, all closely connected to the hydrological cycle and the freshwater budget.[57] The opportunities and challenges associated with the development of cold environments in conjunction with their noticeably rapid response to ongoing climate change raise concerns about the integrity of ecosystems, the sustainability of water resources, and altered hydrological risks under climate change scenarios, hence spur increasing attention from the scientific community and general public.[58] In this regard, Earth system models (ESMs) are used to help with understanding changes in interacting subsystems, elucidating the influence of human activities, and exploring possible future changes.[59] The climate change and climate cycles impacts on

gas hydrate-bearing sediments could be significant causes of uncertainty in projections from ESMs on future effect of climate change, due to the lack of understanding in the processes behind hypothesized serious effects of these sediments on the environment (and thus ecosystems) and their potential to release more greenhouse gases to the atmosphere. In particular, the available models do not account for the presence of hydrates beneath permafrost regions and their potential relation to the permafrost thaw. Also unaccounted for is the threshold temperature at which methane released from hydrates dissociation saturates the capacity of available trapping paths and reaches into the atmosphere. This is partly because there has of yet been no or limited *in situ* experimental research on climate change effects in gas hydrate-bearing permafrost regions. The other principal problems confounding projections of the permafrost thaw are a lack of governing key physics and process understanding. Here, we addressed some of these uncertainties, by combining multi-physics experiments with a series of experiments under realistic conditions. The results of this study could feed into ESMs for better understanding of the effect of climate change on the cold regions. Since the main focus of this study is on the co-existence of ice and hydrates, it can help large scale simulators to quantify the sensitivity to various saturation of ice and hydrates of a modeled permafrost response under imposed retreat. The use of the accurate data we provide here will enhance the accuracy of large-scale simulators, and therefore allow many simulations to have more realistic estimates on the effect of global temperature changes and temperature cycles.

Analysis of the geophysical and geothermal responses of gas hydrate-bearing permafrost sediment samples has also highlighted that the co-existence of hydrates, ice, and unfrozen water in pore space together with the pore-scale temperature-dependent associated phenomena are required to be considered when investigating the potential impacts associated with climate change on permafrost hydrology or the development of cold regions for the energy exploitation. For instance, the simulation packages developed to predict the effect of the environmental temperature change on the hydrological processes in cold environments couple the groundwater flow equation to a heat transfer equation with dynamic freeze-thaw processes, and reliability of the predictions significantly depends on the accuracy of the thermal and hydraulic conductivities considered in the coupled model.[60] Evidenced by our current and previous experimental studies,[5,20] the presence of hydrates in pore space even at low saturations may markedly alter physical properties of the host sediment, particularly at frozen conditions. Therefore, accurate prediction of the evolution of the hydrological processes in permafrost in response to climate change is impossible unless the co-existence of hydrates and ice is incorporated.

Given the expectation of continued global warming over the coming centuries,[61] prediction of the influencing parameters on permafrost thaw and investigation of their social impacts are high priorities for impactful hydrological research. Despite the fact that only 15% of global methane is estimated to be located in hydrate reservoirs, an accountable amount of natural gas hydrates is trapped at shallow depth up to a few hundreds of meters, and they are influenced by the environmental temperature changes.[62] Different geological settings will be affected in a different manner from the naturally occurring ocean and atmosphere temperature cycles on seasonal, decadal, or longer time scales which could cause dissociation and reformation of hydrates. For instance, for deglacial and permafrost hydrates, where ice and hydrate co-exist, warming-induced dissociation can simultaneously happen at both the base and top of the hydrate zone, which are relatively narrow zones in the formation, whereas for most of the marine associated hydrates, the dissociation will occur only at the base of the hydrate zone.[63] This is why geophysical and geomechanical methods applied to characterize the global warming-induced permafrost degradation are required to capture the co-existence of ice and hydrates; otherwise, their response predictions would be erroneous. Monitoring these regions with seismic and thermal conductivity tools combined with the results of our study could make it possible to record the dynamics of gas hydrates and ice-bearing sediments in real environments. Viewing from the energy exploitation angle, quantification of recoverable natural gas accumulated in permafrost settings using the conventional geophysical techniques without considering the co-existence of ice and hydrates would be quite inaccurate unless these methods become coupled with the distinctive approaches such as thermal conductivity measurement.

6. Conclusion

In this study, we explored the geophysical and geothermal responses of simulated gas hydrate-bearing permafrost sediment samples to the temperature change *via* measuring their elastic wave velocities and ETC at different hydrate saturations. We demonstrated that these responses are greatly dependent on the saturation and pore-scale habit of gas hydrates. At sub-zero temperatures, it was indicated that the amount and pore-scale distribution of the unfrozen water content substantially control the evolution of the elastic wave velocities and efficiency of the heat transfer, particularly at the temperatures close to the freezing point. In addition, it was shown how ETC can be used as a distinctive physical property with accounting for the unfrozen water content and distinguishing hydrates from ice at frozen conditions. A conceptual pore-scale model was also proposed for gas hydrate-bearing permafrost sediments based on their geophysical and geothermal responses to the changing temperature. Underpinned by our experimental studies, we discussed that the concerns about the integrity of ecosystems, the sustainability of water resources, and altered hydrological risks in cold regions triggered by the development opportunities or ongoing climate change cannot be understood and accurately predicted unless the co-existence of hydrates, ice, and unfrozen water in pore space and the pore-scale associated phenomena are considered. We believe this work could open a new era in the understanding of how gas hydrate-bearing sediments, particularly those occurring in permafrost settings, respond to the climate change and rise in the environmental temperature. The next step is to modify the available models

and/or develop new pore-scale models with the ability to couple the measured physical properties of gas hydrate-bearing permafrost sediments in order to quantify the saturation and pore-scale distribution of each individual phase.

Conflicts of interest

The authors declare no financial conflicts of interests.

Acknowledgements

The authors would gratefully acknowledge Heriot-Watt University for providing the PhD funding for Mehrdad Vasheghani Farahani through James Watt Scholarship.

References

1 E. D. Sloan Jr and C. A. Koh, *Clathrate Hydrates of Natural Gases*, CRC Press, 2007.

2 A. Hassanpouryouzband, E. Joonaki, M. Vasheghani Farahani, S. Takeya, C. Ruppel, J. Yang, N. J. English, J. M. Schicks, K. Edlmann, H. Mehrabian, Z. M. Aman and B. Tohidi, Gas Hydrates in Sustainable Chemistry, *Chem. Soc. Rev.*, 2020, **49**(15), 5225–5309, DOI: 10.1039/c8cs00989a.

3 E. D. Sloan, Fundamental Principles and Applications of Natural Gas Hydrates, *Nature*, 2003, **426**(6964), 353–359, DOI: 10.1038/nature02135.

4 S. Gupta, B. Wohlmuth and R. Helmig, Multi-Rate Time Stepping Schemes for Hydro-Geomechanical Model for Subsurface Methane Hydrate Reservoirs, *Adv. Water Resour.*, 2016, **91**, 78–87, DOI: 10.1016/j.advwatres.2016.02.013.

5 A. Okwananke, A. Hassanpouryouzband, M. Vasheghani Farahani, J. Yang, B. Tohidi, E. Chuvilin, V. Istomin and B. Bukhanov, Methane Recovery from Gas Hydrate-Bearing Sediments: An Experimental Study on the Gas Permeation Characteristics under Varying Pressure, *J. Pet. Sci. Eng.*, 2019, **180**, 435–444, DOI: 10.1016/j.petrol.2019.05.060.

6 J. Wang, L. Zhang, K. Ge and H. Dong, Capillary Pressure in the Anisotropy of Sediments with Hydrate Formation, *Fuel*, 2021, **289**, 119938, DOI: 10.1016/j.fuel.2020.119938.

7 K. Yamamoto, T. Kanno, X. X. Wang, M. Tamaki, T. Fujii, S. S. Chee, X. W. Wang, V. Pimenov and V. Shako, Thermal Responses of a Gas Hydrate-Bearing Sediment to a Depressurization Operation, *RSC Adv.*, 2017, **7**(10), 5554–5577, DOI: 10.1039/c6ra26487e.

8 Y. Song, L. Zhang, Q. Lv, M. Yang, Z. Ling and J. Zhao, Assessment of Gas Production from Natural Gas Hydrate Using Depressurization, Thermal Stimulation and Combined Methods, *RSC Adv.*, 2016, **6**(53), 47357–47367, DOI: 10.1039/c6ra05526e.

9 M. Vasheghani Farahani, X. Guo, L. Zhang, M. Yang, A. Hassanpouryouzband, J. Zhao, J. Yang, Y. Song and B. Tohidi, Effect of Thermal Formation/Dissociation Cycles on the Kinetics of Formation and Pore-Scale Distribution of Methane Hydrates in Porous Media: A Magnetic Resonance Imaging Study, *Sustainable Energy Fuels*, 2021, **5**(5), 1567–1583, DOI: 10.1039/D0SE01705A.

10 S. D. Kenarsari, D. Yang, G. Jiang, S. Zhang, J. Wang, A. G. Russell, Q. Wei and M. Fan, Review of Recent Advances in Carbon Dioxide Separation and Capture, *RSC Adv.*, 2013, **3**(45), 22739–22773, DOI: 10.1039/c3ra43965h.

11 A. Hassanpouryouzband, J. Yang, B. Tohidi, E. Chuvilin, V. Istomin, B. Bukhanov and A. Cheremisin, Insights into CO2 Capture by Flue Gas Hydrate Formation: Gas Composition Evolution in Systems Containing Gas Hydrates and Gas Mixtures at Stable Pressures, *ACS Sustainable Chem. Eng.*, 2018, **6**(5), 5732–5736, DOI: 10.1021/acssuschemeng.8b00409.

12 A. Hassanpouryouzband, J. Yang, A. Okwananke, R. Burgass, B. Tohidi, E. Chuvilin, V. Istomin and B. Bukhanov, An Experimental Investigation on the Kinetics of Integrated Methane Recovery and CO2 Sequestration by Injection of Flue Gas into Permafrost Methane Hydrate Reservoirs, *Sci. Rep.*, 2019, **9**(1), 1–9, DOI: 10.1038/s41598-019-52745-x.

13 L. Zhang, L. Yang, J. Wang, J. Zhao, H. Dong, M. Yang, Y. Liu and Y. Song, Enhanced CH4 Recovery and CO2 Storage *via* Thermal Stimulation in the CH4/CO2 Replacement of Methane Hydrate, *Chem. Eng. J.*, 2017, **308**, 40–49, DOI: 10.1016/j.cej.2016.09.047.

14 P. Jadhawar, J. Yang, A. Chapoy and B. Tohidi, Subsurface Carbon Dioxide Sequestration and Storage in Methane Hydrate Reservoirs Combined with Clean Methane Energy Recovery, *Energy Fuels*, 2020, **35**(2), 1567–1579, DOI: 10.1021/acs.energyfuels.0c02839.

15 M. T. Reagan and G. J. Moridis, Oceanic Gas Hydrate Instability and Dissociation under Climate Change Scenarios, *Geophys. Res. Lett.*, 2007, **34**(22), DOI: 10.1029/2007GL031671.

16 L. Milich, The Role of Methane in Global Warming: Where Might Mitigation Strategies Be Focused?, *Global Environ. Change*, 1999, **9**(3), 179–201.

17 C. D. Ruppel and J. D. Kessler, The Interaction of Climate Change and Methane Hydrates, *Rev. Geophys.*, 2017, **55**(1), 126–168, DOI: 10.1002/2016RG000534.

18 T. Mestdagh, J. Poort and M. De Batist, The Sensitivity of Gas Hydrate Reservoirs to Climate Change: Perspectives from a New Combined Model for Permafrost-Related and Marine Settings, *Earth-Sci. Rev.*, 2017, **169**, 104–131, DOI: 10.1016/j.earscirev.2017.04.013.

19 R. H. James, P. Bousquet, I. Bussmann, M. Haeckel, R. Kipfer, I. Leifer, H. Niemann, I. Ostrovsky, J. Piskozub, G. Rehder, T. Treude, L. Vielstädte and J. Greinert, Effects of Climate Change on Methane Emissions from Seafloor Sediments in the Arctic Ocean: A Review, *Limnol. Oceanogr.*, 2016, **61**, S283–S299, DOI: 10.1002/lno.10307.

20 J. Yang, A. Hassanpouryouzband, B. Tohidi, E. Chuvilin, B. Bukhanov, V. Istomin and A. Cheremisin, Gas Hydrates in Permafrost: Distinctive Effect of Gas Hydrates and Ice on the Geomechanical Properties of Simulated Hydrate-Bearing Permafrost Sediments, *J. Geophys. Res.: Solid Earth*, 2019, **124**(3), 2551–2563, DOI: 10.1029/2018JB016536.

21 F. Ning, Y. Yu, S. Kjelstrup, T. J. H. Vlugt and K. Glavatskiy, Mechanical Properties of Clathrate Hydrates: Status and Perspectives, *Energy Environ. Sci.*, 2012, **5**(5), 6779–6795, DOI: 10.1039/C2EE03435B.

22 F. E. Nelson, O. A. Anisimov and N. I. Shiklomanov, Climate Change and Hazard Zonation in the Circum-Arctic Permafrost Regions, *Nat. Hazards*, 2002, **26**(3), 203–225, DOI: 10.1023/A:1015612918401.

23 W. F. Waite, J. C. Santamarina, D. D. Cortes, B. Dugan, D. N. Espinoza, J. Germaine, J. Jang, J. W. Jung, T. J. Kneafsey, H. Shin, K. Soga, W. J. Winters and T. S. Yun, Physical Properties of Hydrate-Bearing Sediments, *Rev. Geophys.*, 2009, **47**(4), DOI: 10.1029/2008RG000279.

24 A. I. Best, J. A. Priest, C. R. I. Clayton and E. V. L. Rees, The Effect of Methane Hydrate Morphology and Water Saturation on Seismic Wave Attenuation in Sand under Shallow Sub-Seafloor Conditions, *Earth Planet. Sci. Lett.*, 2013, **368**, 78–87, DOI: 10.1016/j.epsl.2013.02.033.

25 X. Li, Y. Liu, H. Zhang, B. Xiao, X. Lv, H. Yao, W. Pang, Q. Li, L. Yang, Y. Song and J. Zhao, Non-Embedded Ultrasonic Detection for Pressure Cores of Natural Methane Hydrate-Bearing Sediments, *Energies*, 2019, **12**(10), DOI: 10.3390/en12101997.

26 S. Chand, T. A. Minshull, D. Gei and J. M. Carcione, Elastic Velocity Models for Gas-Hydrate-Bearing Sediments—a Comparison, *Geophys. J. Int.*, 2004, **159**(2), 573–590, DOI: 10.1111/j.1365-246X.2004.02387.x.

27 C. Ruppel, Permafrost-Associated Gas Hydrate: Is It Really Approximately 1% of the Global System?, *J. Chem. Eng. Data*, 2015, **60**(2), 429–436, DOI: 10.1021/je500770m.

28 A. Jan and S. Painter, Permafrost Thermal Conditions Are Sensitive to Shifts in Snow Timing, *Environ. Res. Lett.*, 2020, **15**(8), DOI: 10.1088/1748-9326/ab8ec4.

29 M. Vasheghani Farahani, A. Hassanpouryouzband, J. Yang and B. Tohidi, Heat Transfer in Unfrozen and Frozen Porous Media: Experimental Measurement and Pore-Scale Modeling, *Water Resour. Res.*, 2020, **56**(9), DOI: 10.1029/2020WR027885.

30 J. Côté, M.-H. Fillion and J.-M. Konrad, Estimating Hydraulic and Thermal Conductivities of Crushed Granite Using Porosity and Equivalent Particle Size, *J. Geotech. Geoenviron. Eng.*, 2011, **137**(9), 834–842, DOI: 10.1061/(ASCE)GT.1943-5606.0000503.

31 R. G. Ross, P. Andersson and G. Bäckström, Unusual PT Dependence of Thermal Conductivity for a Clathrate Hydrate, *Nature*, 1981, **290**(5804), 322–323, DOI: 10.1038/290322a0.

32 X. Wang, Z. Wang, X. Deng, B. Sun, Y. Zhao and W. Fu, Coupled Thermal Model of Wellbore and Permafrost in Arctic Regions, *Appl. Therm. Eng.*, 2017, **123**, 1291–1299, DOI: 10.1016/j.applthermaleng.2017.05.186.

33 E. Chuvilin and B. Bukhanov, Effect of Hydrate Formation Conditions on Thermal Conductivity of Gas-Saturated Sediments, *Energy Fuels*, 2017, **31**(5), 5246–5254, DOI: 10.1021/acs.energyfuels.6b02726.

34 E. Chuvilin, *Effect of Ice and Hydrate Formation on Thermal Conductivity of Sediments*, ed. B. Bukhanov, IntechOpen, Rijeka, 2018, ch. 7, DOI: 10.5772/intechopen.75383.

35 E. Chuvilin and B. Bukhanov, Thermal Conductivity of Frozen Sediments Containing Self-Preserved Pore Gas Hydrates at Atmospheric Pressure: An Experimental Study, *Geosciences*, 2019, **9**(2), 65, DOI: 10.3390/geosciences9020065.

36 A. Hassanpouryouzband, J. Yang, B. Tohidi, E. Chuvilin, V. Istomin and B. Bukhanov, Geological CO2 Capture and Storage with Flue Gas Hydrate Formation in Frozen and Unfrozen Sediments: Method Development, Real Time-Scale Kinetic Characteristics, Efficiency, and Clathrate Structural Transition, *ACS Sustainable Chem. Eng.*, 2019, **7**(5), 5338–5345, DOI: 10.1021/acssuschemeng.8b06374.

37 ASTM D5334-14, *Standard Test Method for Determination of Thermal Conductivity of Soil and Soft Rock by Thermal Needle Probe Procedure*, ASTM International, West Conshohocken, PA, 2014, DOI: 10.1520/D5334-14.

38 A. Hassanpouryouzband, M. V. Farahani, J. Yang, B. Tohidi, E. Chuvilin, V. Istomin and B. Bukhanov, Solubility of Flue Gas or Carbon Dioxide-Nitrogen Gas Mixtures in Water and Aqueous Solutions of Salts: Experimental Measurement and Thermodynamic Modeling, *Ind. Eng. Chem. Res.*, 2019, **58**(8), 3377–3394, DOI: 10.1021/acs.iecr.8b04352.

39 V. Istomin, E. Chuvilin, B. Bukhanov and T. Uchida, Pore Water Content in Equilibrium with Ice or Gas Hydrate in Sediments, *Cold Reg. Sci. Technol.*, 2017, **137**, 60–67, DOI: 10.1016/j.coldregions.2017.02.005.

40 Y. Dong, J. S. McCartney and N. Lu, Critical Review of Thermal Conductivity Models for Unsaturated Soils, *Geotech. Geol. Eng.*, 2015, **33**(2), 207–221, DOI: 10.1007/s10706-015-9843-2.

41 O. B. Andersland and B. Ladanyi, *An Introduction to Frozen Ground Engineering*, Springer Science & Business Media, 2013. DOI: 10.1007/978-1-4757-2290-1.

42 M. Khurana, Z. Yin and P. Linga, A Review of Clathrate Hydrate Nucleation, *ACS Sustainable Chem. Eng.*, 2017, **5**(12), 11176–11203, DOI: 10.1021/acssuschemeng.7b03238.

43 M. H. Sharqawy, New Correlations for Seawater and Pure Water Thermal Conductivity at Different Temperatures and Salinities, *Desalination*, 2013, **313**, 97–104, DOI: 10.1016/j.desal.2012.12.010.

44 M. J. Assel, J. Millat, V. Vesovic and W. A. Wakeham, The Thermal Conductivity of Methane and Tetrafluoromethane in the Limit of Zero Density, *J. Phys. Chem. Ref. Data*, 1990, **19**(5), 1137–1147, DOI: 10.1063/1.555865.

45 D. D. Cortes, A. I. Martin, T. S. Yun, F. M. Francisca, J. C. Santamarina and C. Ruppel, Thermal Conductivity of Hydrate-Bearing Sediments, *J. Geophys. Res.: Solid Earth*, 2009, **114**(11), DOI: 10.1029/2008JB006235.

46 A. Y. Dandekar, *Petroleum Reservoir Rock and Fluid Properties*, CRC Press, 2nd edn, 2013.

47 B. Ghanbarian and H. Daigle, Thermal Conductivity in Porous Media: Percolation-Based Effective-Medium

Approximation, *Water Resour. Res.*, 2016, **52**(1), 295–314, DOI: 10.1002/2015WR017236.

48 J. Zhao, B. Wang, L. Yang, C. Cheng and Y. Song, A Novel Apparatus for *in Situ* Measurement of Thermal Conductivity of Hydrate-Bearing Sediments, *Rev. Sci. Instrum.*, 2015, **86**(8), 85110, DOI: 10.1063/1.4928106.

49 L. Yang, J. Zhao, B. Wang, W. Liu, M. Yang and Y. Song, Effective Thermal Conductivity of Methane Hydrate-Bearing Sediments: Experiments and Correlations, *Fuel*, 2016, **179**, 87–96, DOI: 10.1016/j.fuel.2016.03.075.

50 G. H. F. Gardner and M. H. Harris, Velocity and Attenuation of Elastic Waves in Sands, *SPWLA 9th Annual Logging Symposium*, Society of Petrophysicists and Well-Log Analysts, 1968.

51 N. Zhang and Z. Wang, Review of Soil Thermal Conductivity and Predictive Models, *Int. J. Therm. Sci.*, 2017, **117**, 172–183, DOI: 10.1016/j.ijthermalsci.2017.03.013.

52 P. Leclaire, F. Cohen-Ténoudji and J. Aguirre-Puente, Extension of Biot's Theory of Wave Propagation to Frozen Porous Media, *J. Acoust. Soc. Am.*, 1994, **96**(6), 3753–3768, DOI: 10.1121/1.411336.

53 P. Serov, A. Portnov, J. Mienert, P. Semenov and P. Ilatovskaya, Methane Release from Pingo-like Features across the South Kara Sea Shelf, an Area of Thawing Offshore Permafrost, *J. Geophys. Res.: Earth Surf.*, 2015, **120**(8), 1515–1529, DOI: 10.1002/2015JF003467.

54 E. A. Amiri, J. R. Craig and B. L. Kurylyk, A Theoretical Extension of the Soil Freezing Curve Paradigm, *Adv. Water Resour.*, 2018, **111**, 319–328, DOI: 10.1016/j.advwatres.2017.11.021.

55 J. M. Frederick and B. A. Buffett, Effects of Submarine Groundwater Discharge on the Present-Day Extent of Relict Submarine Permafrost and Gas Hydrate Stability on the Beaufort Sea Continental Shelf, *J. Geophys. Res.: Earth Surf.*, 2015, **120**(3), 417–432, DOI: 10.1002/2014JF003349.

56 H.-O. Pörtner, D. C. Roberts, V. Masson-Delmotte, P. Zhai, M. Tignor, E. Poloczanska, K. Mintenbeck, M. Nicolai, A. Okem and J. Petzold, *IPCC Special Report on the Ocean and Cryosphere in a Changing Climate*, IPCC Intergov. Panel Clim. Chang., 2019.

57 H. Park, Y. Dibike, F. Su and J. X. Shi, Cold Region Hydrologic Models and Applications, *Arctic Hydrology, Permafrost and Ecosystems*, Springer, 2021, pp. 763–794.

58 O. Aygün, C. Kinnard and S. Campeau, Impacts of Climate Change on the Hydrology of Northern Midlatitude Cold Regions, *Prog. Phys. Geogr. Earth Environ.*, 2019, **44**(3), 338–375, DOI: 10.1177/0309133319878123.

59 R. G. Prinn, Development and Application of Earth System Models, *Proc. Natl. Acad. Sci.*, 2013, **110**(Supplement 1), 3673–3680, DOI: 10.1073/pnas.1107470109.

60 C. Grenier, H. Anbergen, V. Bense, Q. Chanzy, E. Coon, N. Collier, F. Costard, M. Ferry, A. Frampton, J. Frederick, J. Gonçalvès, J. Holmén, A. Jost, S. Kokh, B. Kurylyk, J. McKenzie, J. Molson, E. Mouche, L. Orgogozo, R. Pannetier, A. Rivière, N. Roux, W. Rühaak, J. Scheidegger, J. O. Selroos, R. Therrien, P. Vidstrand and C. Voss, Groundwater Flow and Heat Transport for Systems Undergoing Freeze-Thaw: Intercomparison of Numerical Simulators for 2D Test Cases, *Adv. Water Resour.*, 2018, **114**, 196–218, DOI: 10.1016/j.advwatres.2018.02.001.

61 J. A. Church, P. U. Clark, A. Cazenave, J. M. Gregory, S. Jevrejeva, A. Levermann, M. A. Merrifield, G. A. Milne, R. S. Nerem and P. D. Nunn, *Sea Level Change*, PM Cambridge University Press, 2013.

62 C. D. Ruppel and W. F. Waite, Timescales and Processes of Methane Hydrate Formation and Breakdown, With Application to Geologic Systems, *J. Geophys. Res.: Solid Earth*, 2020, **125**(8), e2018JB016459, DOI: 10.1029/2018JB016459.

63 A. E. Taylor, S. R. Dallimore, P. R. Hill, D. R. Issler, S. Blasco and F. Wright, Numerical Model of the Geothermal Regime on the Beaufort Shelf, Arctic Canada since the Last Interglacial, *J. Geophys. Res.: Earth Surf.*, 2013, **118**(4), 2365–2379, DOI: 10.1002/2013JF002859.